BIOCHEMISTRY
including biophysical chemistry & molecular biology

Article

pubs.acs.org/biochemistry

Distinct Structural and Redox Properties of the Heme Active Site in Bacterial Dye Decolorizing Peroxidase-Type Peroxidases from Two Subfamilies: Resonance Raman and Electrochemical Study

Murat Sezer, Ana Santos, Patrycja Kielb, Tiago Pinto, Ligia O. Martins, and Smilja Todorovic*

Instituto de Tecnologia Química e Biológica, Universidade Nova de Lisboa, Av. da Republica, 2780-157 Oeiras, Portugal

Supporting Information

ABSTRACT: Spectroscopic data of dye decolorizing peroxidases (DyPs) from *Bacillus subtilis* (BsDyP), an A subfamily member, and *Pseudomonas putida* (PpDyP), a B subfamily enzyme, reveal distinct heme coordination patterns of the respective active sites. In solution, both enzymes show a heterogeneous spin population, with the six-coordinated low-spin state being the most populated in the former and the five-coordinated quantum mechanically mixed-spin state in the latter. We ascribe the poor catalytic activity of BsDyP to the presence of a catalytically incompetent six-coordinated low-spin population. The spin populations of the two DyPs are sensitively dependent on the pH, temperature, and physical, i.e., solution versus crystal versus immobilized, state of the enzymes. We observe a redox potential for the Fe^{2+}/Fe^{3+} couple in BsDyP (−40 mV) at pH 7.6 substantially more positive than those reported for the majority of other peroxidases, including PpDyP (−260 mV). Furthermore, we evaluate the potential of the studied enzymes for biotechnological applications on the basis of electrochemical and spectroelectrochemical data.

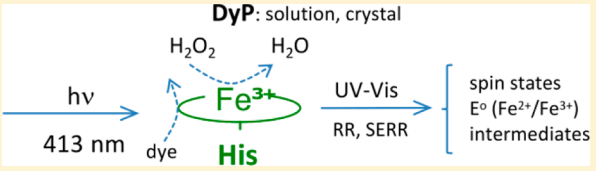

DyP-type peroxidases (DyPs) constitute a family of heme-containing peroxidases.[1−9] Using hydrogen peroxide as an electron acceptor, they are capable of efficient decolorization of numerous dyes, including anthraquinone-based and azo dyes that have industrial and environmental relevance. A comparison of the structural data of DyP-type peroxidases with several representative members of secretory fungal, plant, and bacterial enzymes (i.e., plant peroxidase superfamily) reveals a low level of similarity.[2−8] Unlike classical plant and animal peroxidases, DyPs possess a broad substrate specificity and low pH optima. They lack the distal histidine, which is highly conserved and acts as an acid−base catalyst in the catalytic reaction of classical peroxidases.[10,11] Instead, they house an aspartate within a highly conserved GXXDG distal motif, which in some DyPs plays the role of the distal His. On the proximal side, the heme iron of DyPs is coordinated by a histidine, which is hydrogen-bonded to an acidic residue.[2−9]

On the basis of phylogenetic analysis and catalytic and structural characteristics, DyPs have been classified into four subfamilies, with bacterial enzymes constituting subfamilies A−C and predominantly fungal enzymes belonging to subfamily D.[12] Although a physiological role of DyPs is not fully established, it appears to be subfamily-dependent. In general, the B and C enzymes are predicted to be cytoplasmic, playing therefore a role in intracellular metabolic pathways, while the extracellular A subfamily enzymes are involved in dye degradation and iron uptake.[1,8] Members of the D subfamily, in particular a DyP from plant pathogenic fungus *Thanatephorus cucumeris* Dec1, have been well characterized in terms of substrate specificity, and structure−function relationships.[2,3,9] The studies of bacterial enzymes mainly account for structural data on wild-type and variant proteins from several sources, obtained by X-ray crystallography and electron paramagnetic resonance (EPR) spectroscopy.[2−9] Taken together, emerging evidence indeed underlines the differences between the members of distinct DyP subfamilies. For instance, A subfamily DyPs are generally poorer peroxidases than those from the B subfamily; upon reaction with H_2O_2, compound II is detected in the former and a stable compound I in the latter.[1,4,8,13] Moreover, the A and B subfamily enzymes show significantly different substrate specificities. For instance, DyPB from *Rhodococcus jostii* (and other members of the B subfamily) oxidizes manganese and lignin, whereas DyPA (A subfamily) from the same organism does not.[4] Moreover, fungal DyPs (D subfamily) are highly efficient against anthraquinone dyes but significantly less active toward standard peroxidase substrates and azo dyes.[9] These differences are even more remarkable if we consider analogous primary heme coordination spheres in DyPs. Namely, the two distal residues (Asp and Arg) and the heme-coordinating proximal His are conserved in all DyPs.[2−4,8] The role of these residues, however, appears to be different in distinct DyPs. While the distal Asp was proposed to act as an acid−base catalyst in the D subfamily enzymes,[2,3] it is apparently not crucial for the B subfamily DyPs. The distal Arg244 rather than the Asp153 was found to be essential for the catalytic activity of DyPB,[5] while the latter, together with the distal Asn246, was proposed to modulate the stability (i.e., lifetime) of compound I in this enzyme.[4,5] A substitution of the

Received: December 5, 2012
Revised: April 4, 2013
Published: April 5, 2013

   dx.doi.org/10.1021/bi301630a | *Biochemistry* 2013, 52, 3074−3084

conserved distal Asp residue in the A subfamily enzymes, on the other hand, gave contradictory results with respect to their peroxidase activity.[1,8] Clearly, very subtle structural differences govern significant catalytic divergences of DyPs.

To provide a position for hydrogen peroxide binding, the active site of resting classical peroxidases either has a vacant sixth axial coordination, giving origin to five-coordinated ferric heme iron, or carries a loosely bound water molecule, resulting in a six-coordinated high-spin (HS) configuration.[10,11,14−22] Except for our previous work on PpDyP,[13] the configuration that the heme iron in DyP-type peroxidases adopts in solution (i.e., physiological conditions) has been addressed by only UV−vis absorption spectroscopy, which is insufficiently sensitive for the full characterization of various heme populations that are typically present in heme peroxidases.[2−9] The coordination and spin pattern of DyPs has been frequently discussed on the basis of crystallographic data. However, it is well established that structural features of peroxidase crystals often differ from those in solution, because of the high sensitivity of the active site to physical and chemical conditions.[10,11,19] The recently determined X-ray structure of EfeB/YcdB, an A subfamily DyP from *Escherichia coli*, indicates the presence of a six-coordinated heme iron with a diatomic molecule occupying the sixth axial position.[1] This finding is in contrast to UV−vis absorption data and was attributed to an oxygen-carrying photoreduced ferrous heme iron, produced by a long exposure of the crystals to an X-ray beam.[23] Available structural data for the heme active site of D subfamily enzymes (DyP from fungus *Bjerkandera adusta* Dec1) show the presence of water molecule(s) in the hydrogen peroxide binding pocket.[9] Also, X-ray structural data of DyPB reveal that its heme group carries a solvent molecule in crystal, which is again likely to be a consequence of photoreduction during data collection.[4] Moreover, nonphysiological crystallization conditions, such as a high salt concentration in a buffer solution, may further conceal the true coordination pattern, leading to findings that ions, such as chloride, coordinate the heme iron.[5] The EPR spectroscopic evidence, furthermore, suggests a HS ferric heme in the resting state of DyPB and an additional LS population in DyPA.[4] Nevertheless, a modulation of the active site conformation by packing forces at low temperatures (LT) cannot be excluded in these experiments. Clearly, structural data in solution and physiological-like conditions are required to complement and validate the insights obtained from crystallographic and LT spectroscopic studies. Resonance Raman (RR) spectroscopy has proven to be an especially valuable tool for revealing detailed information about heme coordination and spin state equilibria, cofactor−protein interactions, and catalytic reaction intermediates in classical heme peroxidases.[10] Systematic work on wild-type and mutant peroxidases from different sources led to the establishment of RR spectroscopic markers for specific structural features of resting enzymes and peroxidase intermediates. Detailed structural characterization of a peroxidase in solution state is essential for the rationalization of its catalytic and thermodynamic properties. For instance, the coordination and spin pattern strongly influence the redox potential ($E^{\circ\prime}$) of heme proteins,[24−26] which in peroxidases defines the range of oxidizable substrates.[27] The redox potential of the actual catalytic heme species (compound I/compound II) is difficult to assess experimentally because of the transient nature of the intermediate species. Instead, it can be estimated from the redox potential of the Fe^{2+}/Fe^{3+} couple.[27] Except for the $E^{\circ\prime}_{Fe^{2+}/Fe^{3+}}$ of PpDyP and DyP2 from *Amycolatopsis* sp. 75iv2, there are no available data for the redox properties of DyPs in the literature.[13,28] Surface-enhanced resonance Raman (SERR) spectroelectrochemistry allows for simultaneous characterization of redox, electrocatalytic, and structural properties of immobilized enzymes under working conditions of enzyme-based bioelectronic devices.[13,24,25,29−32]

Here we provide physiologically relevant spectroscopic insights into structural details of active sites of two DyPs from different subfamilies. We present a comparative study of DyPs from *Bacillus subtilis* (BsDyP) and *Pseudomonas putida* (PpDyP), employing RR and SERR spectroscopies that allowed us to correlate the heme coordination patterns of these enzymes in solution, crystal, and immobilized states. We provide the first insights into redox properties of BsDyP and discuss the structural basis for significantly different catalytic and thermodynamic properties of the two enzymes. Taken together, our results contribute to our general understanding of differences that characterize the A and B subfamily DyPs.

MATERIALS AND METHODS

Reagents and Chemicals. 6-Mercaptohexanoic acid, 6-aminohexanethiol hydrochloride, and 8-aminooctanethiol hydrochloride (AOT) were purchased from Dojindo; 6-mercaptohexanol, 11-mercaptoundecanol, 11-mercaptoundecanoic acid, and all other chemicals were purchased from Sigma-Aldrich. For solution measurements, the following buffers were used: Britton-Robinson buffer (pH 5.0), 20 mM Tris-HCl (pH 7.6) containing 0.2 M NaCl, and Britton-Robinson buffer (pH 10.0). For protein immobilization, surface-enhanced resonance Raman (SERR) and chronoamperometry experiments either 12.5 mM potassium phosphate buffer (pH 7.0) containing 12.5 mM K_2SO_4 or acetate buffer (pH 4.5) (20 mM for immobilization; 50 mM with 0.1 M NaCl for experiments) were used. All chemicals were of the highest purity available.

Protein Expression and Purification. Cloning and overexpression of *bsDyP* and *ppDyP* genes in *E. coli* and purification of the expression products followed established procedure.[33] In brief, recombinant strains were grown to an OD_{600} of 0.6 in LB medium containing ampicillin (100 mg/mL). Protein overexpression was induced by addition of 100 μM isopropyl β-D-thiogalactopyranoside (IPTG) to the cell culture in the presence of 15 μM hemin. Once harvested, cells were disrupted with a French press, and cell debris was removed by centrifugation. The resulting supernatants were purified at room temperature, using an ÄKTA system (GE Healthcare Life Sciences). Purification of PpDyP followed a two-step procedure, employing Q-Sepharose and Superdex 200 HR 10/30 columns (GE Healthcare Life Sciences).[33]

Purification of BsDyP followed a three-step procedure, using SP-Sepharose, Mono-S, and Superdex 75 HR 10/30 columns (GE Healthcare Life Sciences).[33]

The protein concentration was determined using a Bradford assay with BSA as a standard along the purification, and the Lambert−Beer law (based on Soret band absorption and an $\varepsilon_{404,PpDyP}$ of 30 mM^{-1} cm^{-1} and an $\varepsilon_{405,BsDyP}$ of 66 mM^{-1} cm^{-1}) for the pure proteins. The protoheme content was determined by the pyridine ferro-hemochrome method, and the heme content was calculated on the basis of the extinction coefficient of pyridine hemochrome *b*.[33] Protein samples with Rz values (A_{406}/A_{280}) of 1.8 for PpDyP and 1.9 for BsDyP were used for subsequent spectroscopic and electrochemical characterizations.

dx.doi.org/10.1021/bi301630a | *Biochemistry* 2013, 52, 3074−3084

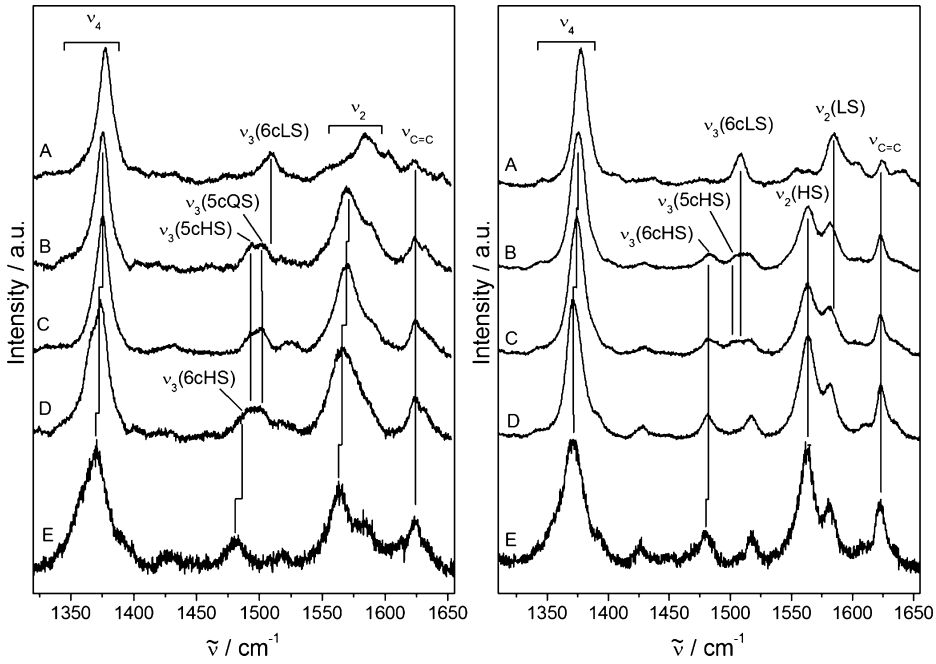

Figure 1. RR spectra of ferric PpDyP and BsDyP measured with 413 nm excitation, at 23 °C. The left panel shows room-temperature RR spectra of the PpDyP−imidazole complex (A) and PpDyP measured at pH 10.0 (B), 7.6 (C), and 5.0 (D) and in the crystal state (E). The right panel shows RR spectra of the BsDyP−imidazole complex (A) and BsDyP measured at pH 10.0 (B), 7.6 (C), and 5.0 (D) and in the crystal state (E). PpDyP and BsDyP crystals were grown at pH 7.3 and 6.5, respectively; a shoulder at 1358 cm^{-1} in the spectrum of the PpDyP crystal (trace E, left) is due to photoreduction.

Sample Preparation. In UV−vis absorption and RR solution experiments, 5−50 μM enzyme was used at desired pH values. SERR and electrochemical measurements of immobilized enzymes were performed using Ag ring electrodes with a geometrical area of 0.75 ± 0.05 cm^2. The electrodes were electrochemically roughened and coated with self-assembled monolayers (SAMs) as described previously.[12] PpDyP was immobilized on a mixed 6-mercaptohexanol/8-aminooctanethiol (3:1, M/M) SAM. The following SAMs were tested for immobilization of BsDyP: pure 6-mercaptohexanol, 6-mercaptohexanoic acid, 11-mercatoundecanoic acid, and 6-mercaptohexanoic acid/6-mercaptohexanol (1:1, M/M), 11-mercaptoundecanoic acid/11-mercaptoundecanol (3:1, M/M), and 6-mercaptohexanol/8-aminooctanethiol (3:1, M/M) mixtures. Immobilization of the DyPs was achieved by immersion of SAM-coated Ag electrodes in a buffer solution containing ∼0.4 mM enzyme for 10−60 min.

BsDyP and PpDyP crystals were grown at room temperature using a 4 μL (2 μL of a 15 mg/mL protein solution with 2 μL of a crystallization solution) hanging drop. The crystallization solution for BsDyP contained 0.25 M magnesium acetate, 0.1 M HEPES (pH 6.5), and 14% (w/v) polyethylene glycol 8000. The crystallization solution for PpDyP contained 0.2 M calcium acetate and 14% (w/v) polyethylene glycol 8000 (pH 7.3).

RR and SERR Spectroscopic Measurements. For low-temperature (−30 to −190 °C) RR experiments, a droplet (2−4 μL) containing either enzyme in solution or enzyme crystals was placed inside a Linkam THMS 600 microscope stage and cooled with liquid N_2. For the room-temperature RR measurements of enzyme crystals, the same sample configuration was used without cooling. Room-temperature RR experiments in solution were taken in a rotating cuvette (from Hellma) filled with ∼80 μL of an ∼50 μM sample, to prevent prolonged exposure of individual enzyme molecules to laser irradiation. Similarly, enzyme-loaded Ag ring working electrodes were rotating at 480 rpm in potential controlled SERR and electrochemical experiments, which were performed using a spectroelectrochemical cell created in house (10 mL volume) equipped with an Ag/AgCl (3 M, KCl) reference electrode (0.21 V vs the standard hydrogen electrode) and a platinum wire counter electrode. Electrode potentials were controlled using a Princeton Applied Research 263A potentiostat; they are referred to the standard hydrogen electrode.

A confocal microscope, equipped with an Olympus 20× objective (working distance of 21 mm, numeric aperture of 0.35), was used for laser focusing onto the sample and light collection in the backscattering geometry. The microscope is coupled to a Raman spectrometer (Jobin Yvon U1000), equipped with a 1200 lines/mm grating and a liquid nitrogen-cooled CCD detector. The 413 nm line from a Kr^+ laser (Coherent Innova 302) was used as the excitation source. The laser power and accumulation time for RR experiments of crystal samples were ∼0.2 mW and 10 s, respectively, and 100 − 200 spectra were co-added to improve the signal:noise ratio. For all other RR and SERR experiments, a 2−3.5 mW laser power was used. In RR experiments, 20−40 spectra, measured with accumulation times of 10−30 s, were co-added in each measurement; in SERR experiments, 3−10 spectra, accumulated for 5−10 s, were co-added. All spectra were subjected to polynomial baseline subtraction and component analysis as described previously[34] using software created in house.

Potentiometric Titration and UV−Vis Absorption Measurements. Potentiometric titrations of BsDyP in solution were performed in an N_2 atmosphere inside a glovebox. Reduction of the ferric enzyme was achieved by stepwise addition of sodium dithionite and monitored by UV−vis spectroscopy. The solution potential was measured with a Ag/AgCl reference electrode, and spectra were recorded using a

dx.doi.org/10.1021/bi301630a | Biochemistry 2013, 52, 3074−3084

Table 1. Putative Assignment of RR Marker Band Modes (ν_i) for 5cHS, 5cQS, 6cHS, and 6cLS Populations in PpDyP and BsDyP, in the Ferric and Ferrous ($^{\#}$) States and upon Formation of the 6cLS−imidazole (6cLS$_{Im}$) Adduct, Determined from the Spectra Recorded at Room Temperature[a]

	PpDyP				BsDyP		
ν_i (cm^{-1})	5cQS	5cHS	6cHS	6cLS/6cLS$_{Im}$	5cHS	6cHS	6cLS/6cLS$_{Im}$
ν_4 ($I_{rel\ \nu_4}$)	1376 (0.63)	1372 (0.29)	1365 (0.06)	1378 (0.02)	1373 (0.22)	1370 (0.35)	1377 (0.43)
		1355$^{\#}$			1355$^{\#}$		
ν_3	1502	1493	1483	1509	1488	1481	1506
		1473$^{\#}$			1471$^{\#}$		
ν_{38}			1518			1517	
ν_2	1572	1565	1559	1585	1565	1563	1582
ν_{37}	1592	1583		1602	1578	1582	
$\nu_{C=C}$	1625	1622		1622	1622	1624	1623
		1624$^{\#}$			1619$^{\#}$		
ν_{10}	1636	1631					1635
ν_{19}	1568	1564			1563		
ν_{11}							1554

[a] $I_{rel\ \nu_4}$ designates the relative intensities of the ν_4 bands observed in RR spectra of the respective ferric DyPs.

Shimadzu UV 1203 spectrophotometer only after stabilization of the potential. The protein concentration was 5 μM in pH 7.6 buffer containing each of the following redox mediators at 2 μM: *N*,*N*-dimethylphenylenediamine (340 mV), 1,2-naphthoquinone-4-sulfonic acid (180 mV), trimethylhydroquinone (115 mV), phenazine methosulfonate (80 mV), phenazine ethosulfonate (55 mV), methylene blue (11 mV), indigo tetrasulfonate, (−30 mV), indigo trisulfonate, (−70 mV), indigo disulfonate, (−110 mV), 2-hydroxy-1,4-naphthoquinone (−152 mV), anthraquinone-2-sulfonic acid (−225 mV), safranine (−280 mV), and neutral red (−325 mV). Redox parameters were obtained by fitting the measured, potential-dependent normalized absorption at 430 nm, which corresponds to the Soret band maximum of the ferrous enzyme, to a Nernst equation. All other UV−vis absorption spectra were recorded using Shimadzu UV 1603 and Nicolet Evolution 300 (Thermo Industries) spectrophotometers.

Chronoamperometry. The electrocatalytic activity of immobilized enzymes was measured by chronoamperometry using the experimental setup for potential-controlled SERR experiments. The poised potential was 0.21 V; the Ag ring electrode rotation was set to 480 rpm to promote mass transport. Currents were recorded as a function of H_2O_2 concentration, which was increased by stepwise injection of a freshly prepared stock solution into the spectroelectrochemical cell. The final H_2O_2 concentrations were 0.2 and 0.9 mM for Bs- and PpDyP, respectively. For each experiment, control measurements were performed with SAM-coated Ag electrodes without the immobilized enzyme.

RESULTS

Influence of the pH, Temperature, and Physical State of the Enzyme on the Spin Population Distribution of Bs- and PpDyPs. When excited into the Soret electronic transition band, resonance Raman (RR) spectra of peroxidases reveal, in the high-frequency region, marker bands sensitive to the spin, oxidation, and coordination state of the heme iron, allowing for a detailed characterization of the active site of the enzymes.[35] In the resting state, RR spectra of Pp- and BsDyPs indicate ferric proteins, as the respective ν_4 bands are found at ∼1375 cm^{-1} (Figure 1, PpDyP in the left panel and BsDyP in the right panel; Table 1). From the inspection of the spin state sensitive ν_3 region of the spectra, it is clear that the heme iron in the two DyPs adopts distinct states and that several spin populations with different coordination patterns coexist in the resting enzymes.

In the solution spectra of PpDyP at pH 7.6 (Figure 1C, left panel), the broad and asymmetric ν_3 band reveals the presence of two major populations, as also supported by component analysis of the spectra (Figure S1 of the Supporting Information). We attribute the ν_3 band at 1493 cm^{-1} to a five-coordinated high-spin (5cHS) population, typically found in the resting state of heme peroxidases.[10,15−22] The position of the other ν_3 band at 1502 cm^{-1} is indicative of both, six-coordinated low-spin (6cLS) and five-coordinated quantum mechanically mixed-spin (5cQS) ferric heme[36] and was previously assigned to the latter.[13] This assignment is supported by electronic absorption spectra that reveal no features of the LS heme group in the resting PpDyP (Figure S2 of the Supporting Information, left panel). Moreover, the vibrational fingerprint of the LS heme, formed upon binding immidazole, a strong ligand, is clearly distinct, showing the ν_3 band at 1509 cm^{-1} (Figure 1A, left panel, and Table 1).

The RR spectra of the resting PpDyP also show broad overlapping bands centered around 1570 cm^{-1}. A component analysis of this region reveals that the main contributions originate from the ν_2 (at 1572 cm^{-1} for QS and 1565 cm^{-1} for the 5cHS population) and ν_{37} (1592 and 1583 cm^{-1} for QS and HS states, respectively) modes. The overlapping bands at higher frequencies are putatively assigned to vinyl stretching (∼1622 cm^{-1}) and ν_{10} (∼1630−1636 cm^{-1}) modes. Deconvolution of the ν_4 region shows that the signal at 1375 cm^{-1} is also composed of two major Lorentzian bands at 1372 and 1376 cm^{-1} (Figure S1 of the Supporting Information), which we attribute to 5cHS and QS species. In addition, a very minor contribution of the 6cHS population (vide infra), with ν_4 at 1365 cm^{-1} and ν_3 at 1483 cm^{-1}, appears to be present in the RR spectra of PpDyP at pH 7.6 (Table 1).

The ν_3 region of RR solution spectra of BsDyP at pH 7.6 (Figure 1C, right panel) also reveals heterogeneous heme coordination, which is different from that in PpDyP. The most obvious differences account for (i) a significant contribution of 6cHS species, as judged by the well-resolved ν_3 mode at 1481 cm^{-1}, and (ii) a complete absence of a QS population. The

dx.doi.org/10.1021/bi301630a | *Biochemistry* 2013, 52, 3074−3084

most populated is the 6cLS state, represented by the ν_3 mode at 1506 cm^{-1} and the ν_2 mode at 1582 cm^{-1}. RR spectra of the 6cLS immidazole−BsDyP complex clearly support this assignment (Figure 1, right panel, trace A, and Table 1). Also, UV−vis spectra of BsDyP show a band at 577 nm, indicative of the LS heme iron (Figure S3 of the Supporting Information, left panel). Moreover, the presence of a CT band at 631 nm suggests a water molecule as the sixth ligand in the 6cHS complex. Component analysis of the entire high-frequency region of the RR spectrum permits identification of the marker bands of 6cLS and 6cHS populations (Table 1 and Figure S1 of the Supporting Information). Furthermore, deconvolution of the BsDyP spectra also suggests minor contributions from the 5cHS heme (with ν_4, ν_3, and ν_2 modes at 1373, 1488, and 1565 cm^{-1}, respectively). The well-resolved vinyl stretching band is positioned at 1623 cm^{-1} and the ν_{10} mode of the 6cLS population at 1635 cm^{-1} (Table 1).

Effect of pH. As also observed for other peroxidases, RR spectra of Bs- and PpDyPs are highly sensitive to the pH of the solution.[10] A careful inspection of the ν_3/ν_2 region in the spectra of the two enzymes (Figure 1B−D, PpDyP in the left panel and BsDyP in the right panel) indicates more pronounced changes in the Bs enzyme. The component analysis of the spectra measured at pH 5 and 10 (Figure S1 of the Supporting Information) could be successfully performed using the same data sets, i.e., band positions and bandwidths, defined for deconvolution of the spectra at neutral pH. As the pH decreases (Figure 1D) toward the optimal pH for the catalytic activity (pH 5 for PpDyP and pH 4 for BsDyP, determined using ABTS as a substrate)[33] in the Bs enzyme, the 6cHS population, with ν_4, ν_3, ν_2, and $\nu_{C=C}$ at 1370, 1481, 1563, and 1624 cm^{-1}, respectively (Figure S1C of the Supporting Information and Table 2), becomes predominant. In PpDyP, we observe a partial conversion of the QS state to the 6cHS state, as the spectral contributions from 6cHS, 5cHS, and QS populations become apparently equal (Figure S1C′ of the Supporting Information and Table 2).

Table 2. Relative Populations of Different Coordination and Spin States in BsDyP and PpDyP as a Function of the pH Value of the Solution, Calculated from the Relative Contribution of the Respective ν_4 Mode

	PpDyP			BsDyP		
	pH 5	pH 7.6	pH 10	pH 5	pH 7.6	pH 10
6cHS	0.30	0.06	0.07	0.68	0.35	0.20
6cLS	0.01	0.02	0.15	0.24	0.43	0.59
5cQS	0.33	0.63	0.51	–	–	–
5cHS	0.36	0.29	0.26	0.08	0.22	0.21

In alkaline media, spectra of both proteins reveal a relative increase in the LS populations (as compared to those at neutral and acidic pH), but neither shows a complete transition to the 6cLS state, as often observed in plant peroxidases.[10,15,20] The RR (Figure S1A,B of the Supporting Information) and UV−vis absorption spectra (Figure S3 of the Supporting Information, left panel) reveal that the LS BsDyP population increases significantly with an increase in pH, apparently at the expense of the 6cHS population (Table 2). The pH dependence of the LS population suggests a hydroxide as the sixth axial ligand at elevated pH. The heme iron of PpDyP appears to bind hydroxide less efficiently, as the QS remains the most abundant population and the LS clearly a minor species at pH 10 (Table 2).

DyPs in Solution versus the Crystal State. To address the influence of the physical state of peroxidase on the spin population distribution in BsDyP and PpDyP, we evaluated RR spectra of single crystals of these enzymes with respect to their solution spectra. Importantly, under the employed experimental conditions (low laser power, short accumulation time, and periodic displacement of the laser beam along the crystal axis), photoreduction is largely avoided, as the RR spectra of crystals show the fingerprint of ferric proteins, particularly in the case of the Bs enzyme (Figure 1E). We observe that small systematic downshifts (2−5 cm^{-1}) of the core size marker bands of the proteins in the crystal state are relatively more pronounced in PpDyP. These shifts are typically associated with a contraction/expansion of the heme pocket,[10,11,19] reflecting, possibly, the more flexible architecture of the PpDyP heme cavity. As expected, the stretching modes of the vinyl substituents do not show a frequency shift. A component analysis of RR spectra of a BsDyP crystal grown at pH 6.5 reveals the 6cHS state as the most abundant and, in addition, the presence of a 6cLS population; the two coordination states are roughly populated as previously observed in solution spectra at pH 5. Some traces of ferrous (photoreduced) enzyme become evident upon deconvolution of the spectra of BsDyP crystals. In the case of the PpDyP crystal, the QS population is completely absent from the spectra. The component analysis of the RR spectrum of the PpDyP crystal (Figure 1E, left panel) reveals contributions from 6cHS and 5cHS ferric species and, with respect to BsDyP, a relatively higher relative contribution of the photoreduced enzyme. This is particularly evident from the broadened ν_4 band, which has a shoulder at 1358 cm^{-1} due to photoreduced heme species. Interestingly, the RR spectra of the crystals show that the 6cHS state is the most populated in both DyPs, as revealed by the ν_3 mode at 1480 cm^{-1} (and ν_2 at 1563 cm^{-1}), which is in clear contrast to solution measurements.

Influence of Temperature. It is well established that the coordination pattern of the heme iron in peroxidases is strongly influenced by temperature,[21] and DyPs are no exception (Figure 2).

Namely, both frequencies of the RR core size marker bands and equilibria of spin and coordination states are highly dependent on temperature.[10,15] This fact actually imposes some limitations on the insights that can be derived from EPR data. In the low-temperature (−190 °C) RR spectra of BsDyP (Figure 2, right panel), we observe upshifted ν_3 bands at 1510 and 1501 cm^{-1}, which can be attributed to 6cLS and 5cHS species, respectively. In addition, as the temperature is lowered, the relative intensity of the ν_3 band of the 6cLS species increases at the expense of that of the respective 5cHS band. Concomitantly, an even more pronounced increase in the relative intensity of the 1585 cm^{-1} band, which contains contributions from the ν_2 (6cLS) and ν_{37} (6cLS) modes, at the expense of the 1563 cm^{-1} band, is observed. These spectral changes are indicative of a conversion of the 5cHS population into the 6cLS population in BsDyP. The 6cHS population, highly abundant at room temperature, does not appear to be sensitive to a decrease in temperature, as the intensity of the ν_3 band at 1481 cm^{-1} does not change as the temperature is decreased (Figure 2, right panel). Moreover, all spectral changes, including small upshifts of the ν_3 (LS) band and downshifts of the ν_3 (6cHS) band, are gradual in the range of studied temperatures for BsDyP. In PpDyP spectra, a sharp

dx.doi.org/10.1021/bi301630a | *Biochemistry* 2013, 52, 3074−3084

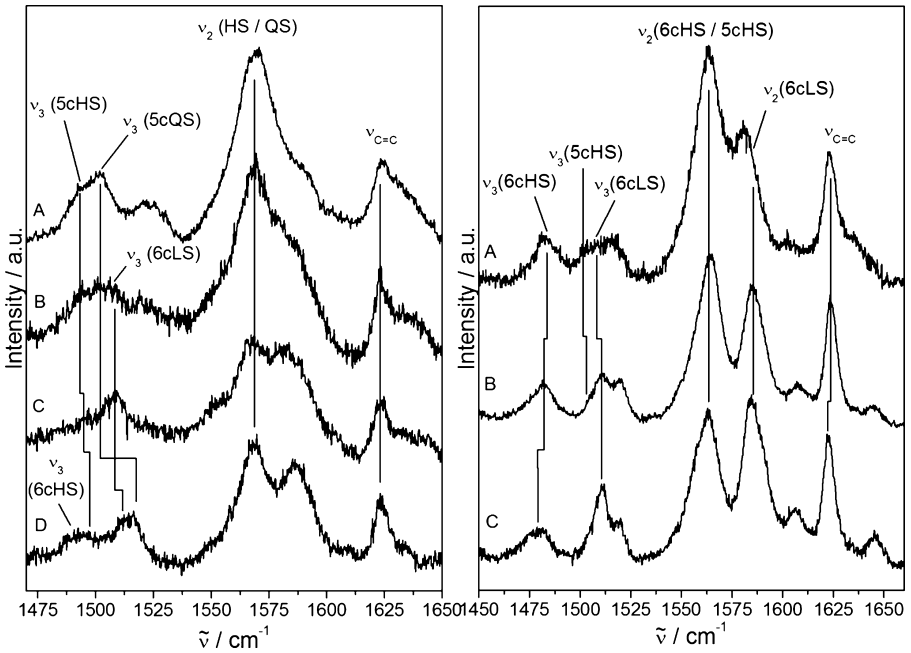

Figure 2. Temperature dependence of spin populations in ferric DyPs. The left panel shows spectra of PpDyP measured at 23 (A), −37.5 (B), −45 (C), and −190 °C (D). The right panel shows spectra of BsDyP measured at 23 (A), −50 (B), and −190 °C (C). Samples were prepared at room temperature in pH 7.6 buffer and measured with 413 nm excitation.

spin transition from the 5cHS to the 6cLS state takes place already at −45 °C (Figure 2C, left panel). As in the case of the Bs enzyme, the 5cHS bands (ν_2 at 1565 cm^{-1} and ν_3 at 1492 cm^{-1}) disappear from PpDyP spectra, while bands characteristic of the 6cLS species (ν_2 at 1585 cm^{-1} and ν_3 at 1509 cm^{-1}) gain intensity (Figure 2, left panel). Until a temperature of −45 °C is reached, the QS population appears to be insensitive to the change in temperature, as its fingerprint bands maintain their relative intensities and frequencies. Interestingly, a further temperature decrease leads to a population of 6cHS species, as indicated by recovery of the signal intensity at 1569 cm^{-1} and an increase in the intensity of the ν_3 band at 1488 cm^{-1} (Figure 2 D, left panel). Moreover, we observe that the frequency of the ν_3 (QS) band upshifts for more than 10 wavenumbers at −190 °C with respect to room temperature. A similar tendency of the QS population was previously reported for barley peroxidase.[15] Taken together, apart from band shifts, the most evident changes in the spectra of Bs- and PpDyPs upon lowering of the temperature account for an increased contribution of the 6cLS species. A similar trend was also observed in the low-temperature RR spectra of crystals of both proteins (data not shown).

Probing Different Spin Populations in Immobilized DyPs. In the next step, we characterized the coordination pattern of BsDyP immobilized onto a biocompatible coated metal support. Surface-enhanced RR (SERR) spectroscopy was employed to probe redox, spin, and coordination states of the immobilized enzyme,[13,24,25,29−32] and coupled to electrochemical methods, to provide information about the redox and catalytic properties of the adsorbed enzyme. This approach is particularly informative for the investigation of the potential of peroxidases for biotechnological applications, as it simultaneously reveals structural features and monitors the overall catalytic activity, electronic coupling, and redox transitions of immobilized proteins under working conditions of bioelectronic devices. We have shown previously that PpDyP could be adsorbed onto solid Ag electrodes coated with an alkanethiol self-assembled monolayer (SAM),[13] under preservation of the solution coordination pattern(s) and redox properties (Figure S2 of the Supporting Information, right panel).

A similar strategy was adopted here to immobilize BsDyP in the native and simultaneously electroactive state. Pure and mixed methyl-, carboxyl-, hydroxyl-, and amino-terminated alkanethiols and different incubation and measuring buffers were tested. Clearly, the two studied DyPs reveal a distinct surface charge distribution: while PpDyP adsorbs onto biocompatible surfaces with a "diluted" positive charge,[13] indicating the presence of negatively charged residues on its surface, BsDyP requires negatively charged carboxyl-terminated SAM coating for immobilization. However, immobilzation of BsDyP was only partially successful, as revealed by the comparison of the solution (RR) spectra and SERR spectra of the immobilized enzyme.

At a given pH value, we observe an increased 6cLS:6cHS ratio in the case of the immobilized BsDyP compared to that of the solution state. This points toward a high sensitivity of the BsDyP heme pocket to electric fields at the electrode surface,[24,29,37] and/or the effect of an altered local pH at the SAM−solution interface.[24,37] Moreover, reduction of the immobilized BsDyP was never fully accomplished (Figure 3C). Redox sensitive spectral changes were observed only until a decrease of the poised potential to −100 mV. Below this value, the relative amount of reduced enzyme remained the same, even at the most negative potential applicable to the alkanethiol-coated Ag electrodes (approximately −490 mV). The best results were obtained employing pure carboxyl-terminated SAMs for protein immobilization at pH 4.5 (Figure 3). Under these immobilization conditions, the core size marker bands of BsDyP appear at the same frequencies, with unchanged bandwidths, and comparable relative intensities in RR and SERR spectra (Figure 3A and Figure 1D, right panel).

dx.doi.org/10.1021/bi301630a | Biochemistry 2013, 52, 3074−3084

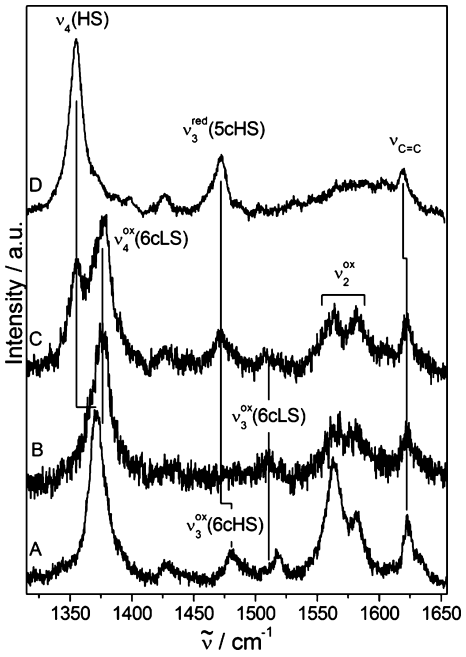

Figure 3. SERR and RR spectra of BsDyP. (A–C) SERR spectra of BsDyP immobilized on a 6-mercaptohexanoic acid SAM (pH 4.5) measured (A) at open circuit (278 mV), (B) at 210 mV in the presence of 0.1 mM H_2O_2, and (C) at a poised potential of −90 mV. (D) RR spectrum of dithionite-reduced BsDyP (pH 7.6).

As in solution at pH ≤5, the ferric BsDyP adopts mainly the 6cHS configuration (vide supra); however, contributions from 6cLS species become higher upon immobilization. The portion of immobilized BsDyP that is electrochemically reducible is, nevertheless, in the native state, as we concluded from the comparison of the SERR spectra with the RR spectrum of the dithionite-reduced BsDyP in solution (Figure 3C,D). The spectra show prominent ν_4, ν_3, and $\nu_{C=C}$ bands at 1355, 1471, and 1619 cm^{-1}, respectively, characteristic of a single ferrous 5cHS species (Figure 3D), as previously reported for ferrous PpDyP.[13] Reversible reduction of the 6cHS population of immobilized BsDyP occurs between 0 and −100 mV, as the protein returns to the fully oxidized state upon application of the positive potential to the electrode. Moreover, the redox inactive ferric population bears the fingerprint of the LS population as revealed by component analysis of the SERR spectra.

Addition of hydrogen peroxide to the ferric immobilized BsDyP failed to provide any detectable SERR signal indicative of formation of compound II, although UV–vis absorption data suggest that this intermediate is formed in solution (Figure S3 of the Supporting Information). Namely, upon reaction with H_2O_2, the Soret and Q- bands of the resting state at 406, 504, and 538 nm red-shift to 416, 526, and 554 nm, respectively, and the CT band at 631 nm becomes less intense and downshifts to ∼620 nm. The intermediate has a half-life time ($\tau_{1/2}$) of ∼12 min at pH 7.6 and spontaneously decays back to the resting state (Figure S3 of the Supporting Information, right panel). We have previously observed that PpDyP forms a stable compound I-like species ($\tau_{1/2}$ ∼ 60 min).[13] However, we were unable to detect any intermediate species by SERR or RR spectroscopy in either enzyme. The SERR spectrum of ferric BsDyP in the presence of hydrogen peroxide is, nevertheless, remarkable as it reveals a fingerprint of a stable, "nonreacted" ferric 6cLS population that appears to be unaffected by the presence of H_2O_2 (Figure 3B). This finding suggests that the 6cLS BsDyP population represents a species that is locked in an unfavorable coordination that is at the same time redox inactive and catalytically incompetent, because it does not allow for substrate binding. Furthermore, this interpretation is in line with UV–vis data for BsDyP, which reveal the appearance of a shoulder at 577 nm, indicative of the LS population, upon addition of 1.1 equiv of H_2O_2 (Figure S3 of the Supporting Information).

Redox and Catalytic Properties of DyPs. Except for data for PpDyP[13] and C-type DyP2 from *Amycolatopsis* sp. 75iv2,[28] there are no reports of redox properties of any other DyP-type peroxidase. We measured the redox potential of the Fe^{2+}/Fe^{3+} couple of BsDyP, first in solution and then in the immobilized state.

The potentiometric titration of BsDyP in solution at pH 7.6 reveals a redox transition at $E^{\circ\prime}_{Fe^{2+}/Fe^{3+}}$ ∼ −40 mV and an apparent number of transferred electrons (n_{app}) of ∼0.7 (Figure 4). The transition is broad, possibly reflecting close, unresolved

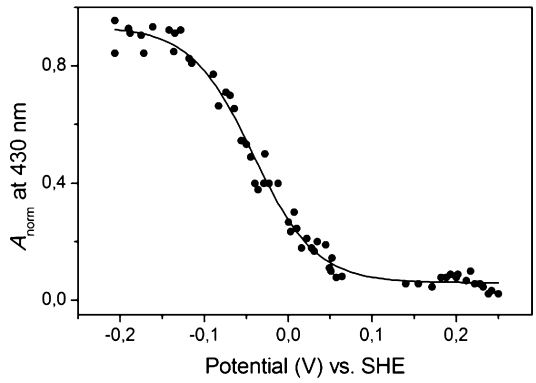

Figure 4. Potentiometric redox titration of BsDyP in solution at pH 7.6 followed by UV–vis spectroscopy. A sigmoid function (—) is fit to the potential-dependent normalized absorption (A_{norm}) at 430 nm (●) for two separate experiments.

redox potentials of different heme species. In the next step, we addressed the redox properties of the electroactive portion of immobilized BsDyP by potential-dependent SERR spectroscopy. Analysis of the spectra measured at different poised potentials applied to the working electrode[13,24,25,29–31] allowed for an estimation of the redox potential of the "functional" 6cHS population of immobilized BsDyP to a value between 0 and −0.1 V at pH 4.5. The 6cLS portion could not be electrochemically reduced and therefore was not considered in the analysis. It is interesting to note that the redox transitions of both immobilized and solution BsDyP are by more than 0.2 V higher than the respective values for PpDyP ($E^{\circ\prime}_{Fe^{2+}/Fe^{3+}solution}$ = −260 mV, n_{app} =1, $E^{\circ\prime}_{Fe^{2+}/Fe^{3+}imm}$ = −300 mV).[13]

Furthermore, we previously demonstrated an efficient electrocatalysis of the immobilized PpDyP in the presence of H_2O_2 by chronoamperometry.[13] A similar approach was adopted here to characterize the electrocatalytic activity of immobilized BsDyP. As in the experiments with PpDyP, a H_2O_2-dependent electrocatalytic reduction current was measured at a poised potential of 210 mV. At this potential noncatalytic H_2O_2 reduction can be excluded. In fact, negative currents measured upon addition of H_2O_2 indicate catalytic activity of BsDyP (Figure 5); however, the magnitude of the currents is lower for BsDyP by 2 orders of magnitude than for

dx.doi.org/10.1021/bi301630a | *Biochemistry* 2013, 52, 3074–3084

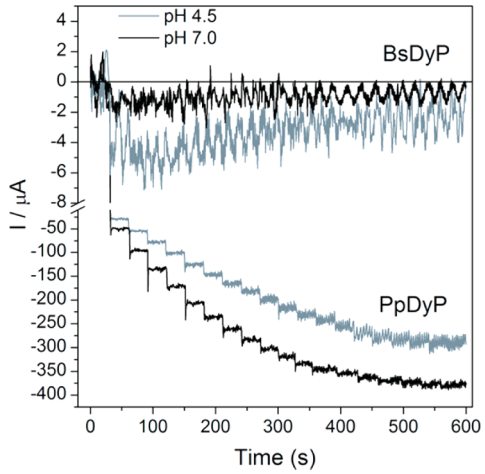

Figure 5. Electrocatalytic activity of BsDyP (top traces) and PpDyP (bottom traces) at pH 4.5 and 7. The poised electrode potential was 210 mV, and every 30 s aliquots of 10 and 50 μM H_2O_2 were added to the spectroelectrochemical cell containing immobilized BsDyP and PpDyP, respectively.

PpDyP. On the other hand, while the apparent Michaelis–Menten constant for immobilized PpDyP ($K_{M,app}$) was 220 ± 25 μM,[13] the respective value for BsDyP is lower by ~2 orders of magnitude, as the maximal electrocatalytic current has already been reached after the first injection of only 10 μM H_2O_2 (Figure 5). Moreover, the catalytic incompetence of the 6cLS species, which is significantly abundant at neutral (and basic) pH, is also reflected in chronoamperograms, as we observe a higher electrocatalytic activity of the immobilized BsDyP at pH 4.5 compared to that at pH 7.0 (Figure 5).

DISCUSSION

DyPs are enzymes that efficiently degrade a wide range of dyes. Understanding their structural, thermodynamic, and biochemical features is of utmost interest from perspectives of both fundamental and applied science. Herein, we present a detailed comparative study of structural and redox properties of members of DyP subfamilies A and B (BsDyP and PpDyP, respectively) that helped us rationalize their different catalytic behavior.[33] In addition, our results shed some light onto the potential for utilization of the respective immobilized DyPs in the development of biotechnological devices.

BsDyP and PpDyP Adopt Heterogeneous and Distinct Heme Configurations in Solution. This solution resonance Raman study reveals several coexisting spin populations in resting Bs- and PpDyPs. A heterogeneous spin population is actually quite common for bacterial and plant peroxidases, as a mixture of 6cHS and 5cHS populations was observed in resting states of CCP, HRP, and SBP, among others.[18,20,22]As in other peroxidases, the relative abundance of different spin states in Bs- and PpDyPs is dependent on the temperature, pH value of the solution, and physical state of the enzyme.[10] A change in any of these parameters induces a typically reversible interconversion of the spin populations. However, we observe very different spin states in the two studied enzymes. This is an unexpected finding, having in mind that the structural models of the respective active sites suggest that the first coordination sphere of the heme iron is highly analogous in both enzymes.[33] The two conserved residues on the distal side [Asp132 (Asp240 for BsDyP) and Arg214 (Arg339 for BsDyP) for PpDyP] and the proximal His (His197 and His326 for Pp- and BsDyP, respectively) residue are located and oriented in a comparable manner with respect to the heme iron. According to the model, the third distal residue, proposed to modulate the reactivity of DyPs,[5] is also the same (Asn136 and Asn244 for Pp- and BsDyP, respectively) in the two enzymes. The main difference between the model structures, however, accounts for the distance between the proximal His and Asp, which is shorter in PpDyP than in BsDyP.[33] A shorter His–Asp distance would imply a stronger hydrogen bond between these residues, resulting in greater imidazolate character of the proximal His.[10,22] As a consequence, the Fe–His bond length would be shorter, and the Fe ion would be pulled out of the heme plane to a greater extent in PpDyP than in BsDyP. In fact, this would explain why the Fe ion in PpDyP binds distal ligands (H_2O or OH) less readily than BsDyP. Accordingly, mainly five-coordinate species are present in PpDyP and six-coordinate species in BsDyP. However, differences between spectroscopic and model-derived structural data may also be related to the highly flexible heme pockets, which indicate that structural insights provided by static models of DyPs have to be considered as an approximation. Under physiological conditions, the dynamic nature of the heme pocket appears to be crucial for understanding the structural and mechanistic properties of DyPs. Accordingly, RR spectra of BsDyP and PpDyP in the crystal state, which reflects better the static nature of the model structures, point to comparable coordination patterns and indicate 6cHS as the main species in both enzymes.

Resting BsDyP Favors the Catalytically Incompetent 6cLS Configuration; Resting PpDyP Is Predominantly in the QS State. Recent studies of two bacterial DyPs from *R. jostii* RHA1, which, according to the phylogenetic analysis, belong to different subfamilies, support subfamily-dependent properties of DyPs.[4,5] The structural and kinetic data of DyPA and DyPB reveal significant differences in the type of stabilized catalytic intermediates, peroxidase activities, and specific heme microenvironments in the two enzymes.[4,5] EPR studies suggest that in DyPA the major HS population with a rhombic symmetry coexists with a significant amount of LS species. The active site in DyPB is characterized by a rhombically distorted axial symmetry, indicating the 6cHS coordination.[4] Here, we provide UV–vis and RR spectroscopic evidence that the LS population is present in BsDyP at pH 7.6 and room temperature. Interestingly, UV–vis spectra of another member of subfamily A, TfuDyP, are also indicative of the LS population.[8] It is tempting to correlate the presence of LS species with general structural characteristics of subfamily A DyPs; however, solid conclusions require more data for other members of the subfamily. This finding is nevertheless unexpected, because the LS species does not allow for efficient substrate binding and therefore results in a catalytically incompetent peroxidase. We demonstrate here that the 6cLS population indeed remains present and unaltered in SERR spectra of BsDyP in the presence of H_2O_2. Moreover, the decrease in the amount of the 6cLS species upon lowering the pH is directly correlated with an increased catalytic current in chronoamperometric experiments. At this point, neither the molecular origin of the 6cLS species nor the nature of the sixth ligand coordinating the heme iron in BsDyP is clear. Nevertheless, the highly flexible heme cavity in peroxidases, in general, facilitates formation of the LS state in a pH-dependent manner. Recombinant HRP in which the distal His

dx.doi.org/10.1021/bi301630a | *Biochemistry* 2013, 52, 3074–3084

was substituted with an Arg undergoes a partial spin conversion into a 6cLS species.[38] In manganese peroxidase and ferrous HRP, LS states can be generated in variants carrying point mutations in the second coordination sphere at the proximal side.[18] The conformational perturbation in these proteins therefore propagates to the distal side of the heme and induces the formation of LS species. Also, mutation of the distal Arg244 to Leu in DyPB caused a pH-dependent transition from a HS to a LS state and abolishment of peroxidase activity in this enzyme.[5] Similarly, a poor catalytic activity of DyPB was observed when Asp153 was replaced with histidine, in an attempt to engineer a plant peroxidase-like distal heme cavity. The X-ray structure of this variant reveals the (excessive) proximity of the Nε2 atom to the heme iron (1.8 Å shorter than the Fe−His42 bond in HRP), likely favoring the LS configuration.[5]

Surprisingly, the major population of PpDyP, at room temperature and pH 7.6, is in the QS state. This is a curious result, bearing in mind that this spin state mixture of intermediate-spin ($S = {}^3/_2$) and HS iron was originally described only in class III plant peroxidases[20] and cytochromes c'.[36] Nevertheless, it was recently also observed in Kat G catalase-peroxidase,[39] indicating that it might be more widespread in heme proteins than previously believed.

The Redox Potential of BsDyP Is Relatively High. Heme peroxidases typically reveal negative redox potentials of the Fe^{2+}/Fe^{3+} couple.[40] This experimentally easily measurable parameter is considered to be a good estimation of redox properties of the catalytically relevant redox couples, because the molecular factors influence both in the same manner.[27] Therefore, a higher $E^{\circ\prime}_{Fe^{2+}/Fe^{3+}}$ most likely implies a higher redox potential of compound I/compound II and compound II/Fe^{3+} couples. The Pp- and BsDyPs show clearly distinct redox potentials. A significantly higher redox potential of BsDyP ($E^{\circ\prime}_{Fe^{2+}/Fe^{3+}} = -40$ mV) would suggest that it is a more efficient peroxidase with a broader range of oxidizable substrates than PpDyP ($E^{\circ\prime}_{Fe^{2+}/Fe^{3+}} = -260$ mV). The $K_{M,sol}$ value for BsDyP for hydrogen peroxide (7 ± 1 μM) is much lower than the respective value for PpDyP (79 ± 5 μM), using ABTS as the substrate.[33] The significantly lower K_M value may reflect a higher affinity of BsDyP for hydrogen peroxide compared to that of PpDyP. For these substrates, BsDyP is in fact more efficient than PpDyP despite a significantly lower turnover [V_{max}(BsDyP)/V_{max}(PpDyP) ∼ 0.6]. However, for more than 20 other dyes and phenolic and nonphenolic compounds tested, the turnover and efficiency of PpDyP are up to 2 orders of magnitude higher than those of BsDyP.[33] One possible reason for the poorer catalytic performance of BsDyP lies in its overall structural features. Namely, structural data of DyPB reveal the presence of two access routes of solvent/substrate molecules to the active site: through the distal channel and via the propionate pocket.[4,5] Moreover, a comparison of the available structures suggests that the residues that line the distal channel are conserved in B and D subfamily enzymes. However, this channel, which might be a determinant for substrate specificity, is blocked in the A subfamily DyPs.[4] Our data point to structural features of the heme iron as an additional factor for the poor catalytic activity of BsDyP, as they reveal the presence of a significant amount of the catalytically incompetent six-coordinated LS population in this enzyme (vide supra).

Immobilized BsDyP Shows Poor Electrocatalytic Activity. The immobilized PpDyP shows significantly better catalytic performance than the immobilized BsDyP, as judged by the measured catalytic currents in the presence of H_2O_2, employing chronoamperometry, that are 2 orders of magnitude higher for the former. On one hand, this finding reflects an intrinsically higher rate of turnover of PpDyP compared to that of BsDyP, as also observed for the enzymes in solution. On the other hand, the catalytically incompetent 6cLS portion of BsDyP increases upon immobilization. We have shown that PpDyP represents a promising candidate for construction of a bioelectronic device(s) with the unique DyP-type peroxidase substrate specificity,[13] as it retains the solution native structure and promotes efficient electronic coupling to the electrode with no significant modulation of the redox potential with respect to the solution value. The immobilized BsDyP does not share these properties and most likely does not have noteworthy potential in the field of applied science. This finding may in fact reflect a general characteristic of the A subfamily members of DyPs.[4,5]

■ CONCLUSIONS

In conclusion, herein we demonstrate that the two studied DyP peroxidases possess some characteristics that are common to classical peroxidases, but they also reveal a number of particularities. In the absence of detailed spectroscopic and thermodynamic data for other DyPs, it is difficult to say at this point if these differences reflect general, subfamily-related features. In the reaction with hydrogen peroxide, BsDyP and PpDyP behave as typical members of subfamilies A and B,[1,4,5,12] stabilizing the compound II and compound I intermediates, respectively. Both PpDyP and BsDyP possess a highly flexible heme cavity, revealing heterogeneous but distinct spin populations, sensitive (in different manners) to the temperature, pH, and physical state of the protein. Nevertheless, the 5cHS and 6cHS states, which are in classical peroxidases predominant, are minor species in the studied DyPs at neutral pH. Instead, the 6cLS and 5cQS states are in solution at pH 7.6 the most populated in BsDyP and PpDyP, respectively. The axial coordination and the polarity of the immediate heme environment further influence the redox properties of heme proteins. Actually, we observe substantially more positive redox potential of the Fe^{2+}/Fe^{3+} couple in BsDyP (−40 mV) at pH 7.6 compared to those reported for a majority of other peroxidases, [27] which is, nevertheless, comparable with the value for the recently characterized DyP2 from *Amycolatopsis* sp. 75iv2 (−85 mV).[28] The redox potential of PpDyP (−260 mV), on the other hand, falls into the range of values typically observed in classical peroxidases. Furthermore, our previous work on immobilized PpDyP revealed that it has a high potential for construction of enzyme-based biosensors and biocatalysts, as it shows structural integrity and electrocatalytic activity in the immobilized state.[13] Here we show that BsDyP could not be immobilized on biocompatible metal supports with preservation of the native structure and catalytic activity. Being, at the same time, a less efficient peroxidase, BsDyP represents a poor choice for biotechnological applications. Taken together, our results contribute to a better understanding of DyP-type peroxidases in general and highlight the differences in the active site structure in members of DyP subfamilies A and B that may underlie their distinct catalytic properties.

dx.doi.org/10.1021/bi301630a | *Biochemistry* 2013, 52, 3074−3084

■ ASSOCIATED CONTENT

Supporting Information

Component analysis of RR spectra of PpDyP and BsDyP (Figure S1), electronic absorption and (SE)RR spectra of PpDyP (Figure S2), and electronic absorption spectra of ferric and ferrous BsDyP in the presence and absence of imidazole and H_2O_2 (Figure S3). This material is available free of charge via the Internet at http://pubs.acs.org.

■ AUTHOR INFORMATION

Corresponding Author

*Phone: (+351) 21 4469717. E-mail: smilja@itqb.unl.pt.

Funding

Financial support from FCT Grant PTDC/BIA-PRO/100791/2008 to S.T. is gratefully acknowledged.

Notes

The authors declare no competing financial interest.

■ ACKNOWLEDGMENTS

We thank Daniela Presa for critical reading of the manuscript.

■ ABBREVIATIONS

DyP, dye decolorizing peroxidase; HS, high-spin; LS, low-spin; QS, quantum mechanically mixed-spin; 5c, five-coordinated; 6c, six-coordinated; (SE)RR, (surface-enhanced) resonance Raman; ABTS, 2,2′-azinobis(3-ethylbenzothiazoline-6-sulfonic acid); SAM, self-assembled monolayer.

■ REFERENCES

(1) Liu, X., Du, Q., Wang, Z., Zhu, D., Huang, Y., Li, N., Wei, T., Xu, S., and Gu, L. (2011) Crystal Structure and Biochemical Features of EfeB/YcdB from *Escherichia coli* 0157. *J. Biol. Chem. 286*, 14922−14931.

(2) Sugano, Y., Muramatsu, R., Ichiyanagi, A., Sato, T., and Shoda, M. (2007) DyP, a Unique Dye-decolorizing Peroxidase, Represents a Novel Heme Peroxidase Family: Asp^{171} Replaces the Distal Histidine of Classical Peroxidases. *J. Biol. Chem. 282*, 36652−36658.

(3) Sugano, Y. (2009) DyP-type Peroxidases Comprise a Novel Heme Peroxidase Family. *Cell. Mol. Life Sci. 66*, 1387−1403.

(4) Roberts, J. N., Singh, R., Grigg, J. C., Murphy, M. E. P., Bugg, T. D. H., and Eltis, L. D. (2011) Characterization of Dye-Decolorizing Peroxidases from *Rhodococcus jostii* RHA1. *Biochemistry 50*, 5108−5119.

(5) Singh, R., Grigg, J. C., Armstrong, Z., Murphy, M. E. P., and Eltis, L. D. (2012) Distal Heme Pocket Residues of B-type Dye-decolorizing Peroxidase: Arginine but not Aspartate is Essential for Peroxidase Activity. *J. Biol. Chem. 287*, 10623−10630.

(6) Zubieta, C., Sri Krishna, S., Kapoor, M., Kozbial, P., McMullan, D., Axelrod, H. L., Miller, M. D., Abdubek, P., Ambing, E., Astakhova, T., Carlton, D., Chiu, H.-J., Clayton, T., Deller, M. C., Duan, L., Elsliger, M.-A., Feuerhelm, J., Grzechnik, S. K., Hale, J., Hampton, E., Won Han, G., Jaroszewski, L., Jin, K. K., Klock, H. E., Knuth, M. W., Kumar, A., Marciano, D., Morse, A. T., Nigoghossian, E., Okach, L., Oommachen, S., Reyes, R., Rife, C. L., Schimmel, P., van der Bedem, H., Weeks, D., White, A., Xu, Q., Hodgson, K. O., Wooley, J., Deacon, A. M., Godzik, A., Lesley, S. A., and Wilson, I. A. (2007) Crystal Structures of two Novel Dye-decelorizing Peroxidases Reveal a β-barrel Fold with a Conserved Heme-binding Motif. *Proteins 69*, 223.

(7) Zubieta, C., Joseph, R., Sri Krishna, S., McMullan, D., Kapoor, M., Axelrod, H. L., Miller, M. D., Abdubek, P., Acosta, C., Astakhova, T., Carlton, D., Chiu, H.-J., Clayton, T., Deller, M. C., Duan, L., Elias, Y., Elsliger, M.-A., Feuerhelm, J., Grzechnik, S. K., Hale, J., Won Han, G., Jaroszewski, L., Jin, K. K., Klock, H. E., Knuth, M. W., Kozbial, P., Kumar, A., Marciano, D., Morse, A. T., Murphy, K. D., Nigoghossian, E., Okach, L., Oommachen, S., Reyes, R., Rife, C. L., Schimmel, P., Trout, C. V., van der Bedem, H., Weeks, D., White, A., Xu, Q., Hodgson, K. O., Wooley, J., Deacon, A. M., Godzik, A., Lesley, S. A., and Wilson, I. A. (2007) Identification and Structural Characterization of Heme Binding in a NOvel Dye-decolorizing Peroxidase, TyRA. *Proteins 69*, 234−243.

(8) van Bloois, E., Torres Pazmino, D. E., Winter, R. T., and Fraaije, M. W. (2010) A Robust and Extracellular Heme-containing Peroxidase from *Thermobifida fusca* as Prototype of a Bacterial Peroxidase Superfamily. *Appl. Microbiol. Biotechnol. 86*, 1419−1430.

(9) Kim, S. J., and Shoda, M. (1999) Purification and Characterization of a Novel Peroxidase from *Geotrichum candidum* Dec 1 Involved in Decolorization of Dyes. *Appl. Environ. Microbiol. 65*, 1029−1035.

(10) Smulevich, G., Feis, A., and Howes, B. D. (2005) Fifteen Years of Raman Spectroscopy of Engineered Heme Containing Peroxidases: What Have We Learned? *Acc. Chem. Res. 38*, 433−440.

(11) Henriksen, A., Mirza, O., Indiani, C., Teilum, K., Smulevich, G., Welinder, K. G., and Gajhede, M. (2001) Structure of Soybean Seed Coat Peroxidase. *Protein Sci. 10*, 108−115.

(12) Ogola, H. J. O., Kamiike, T., hashimoto, N., Ashida, H., Ishikawa, T., Shibata, H., and Sawa, Y. (2009) Molucular Characterization of a Novel Peroxidase from the Cyanobacterium *Anabena* sp. strain PCC 7120. *Appl. Environ. Microbiol. 75*, 7509.

(13) Sezer, M., Genebra, T., Mendes, S., Martins, L. O., and Todorovic, S. (2012) A DyP-type Peroxidase at a Bio-compatible Interface: Structural and Mechanistic Insights. *Soft Matter 8*, 10314−10321.

(14) Feis, A., Howes, B. D., Indiani, C., and Smulevich, G. (1998) Resonance Raman and Electronic Absorption Spectra of Horseradish Peroxidase Isozyme A2: Evidence for a Quantum-mixed Spin Species. *J. Raman Spectrosc. 29*, 933−938.

(15) Howes, B. D., Schiodt, C. B., Welinder, K. G., Marzocchi, M. P., Ma, J.-G., Zhang, J., Shelnutt, J. A., and Smulevich, G. (1999) The Quantum Mixed-Spin Heme State of Barley Peroxidase: A Paradigm for Class III Peroxidases. *Biophys. J. 77*, 478−492.

(16) Howes, B. D., Brissett, N. C., Doyle, W. A., Smith, A. T., and Smulevich, G. (2005) Spectroscopic and Kinetic Properties of the Horseradish Peroxidase Mutant T171S. *FEBS J. 272*, 5514−5521.

(17) Howes, B. D., Rodriguez-Lopez, J. N., Smith, A. T., and Smulevich, G. (1997) Mutation of Distal Residues of Horseradish Peroxidase: Influence on Substrate Binding and Cavity Properties. *Biochemistry 36*, 1532−1543.

(18) Howes, B. D., Feis, A., Raimondi, L., Indiani, C., and Smulevich, G. (2001) The Critical Role of the Proximal Calcium Ion in the Structural Properties of Horseradish Peroxidase. *J. Biol. Chem. 276*, 40704−40711.

(19) Indiani, C., Santoni, E., Becucci, M., Boffi, A., Fukuyama, K., and Smulevich, G. (2003) New Insights into the Peroxidase-Hydroxamic Acid Interaction Revealed by Combination of Spectroscopic and Crystallographic Studies. *Biochemistry 42*, 14066−14074.

(20) Nissum, M., Feis, A., and Smulevich, G. (1998) Characterization of Soybean Seed Coat Peroxidase: Resonance Raman Evidence for a Structure-based Classification of Plant Peroxidases. *Biospectroscopy 4*, 355−364.

(21) Smulevich, G., and Spiro, T. G. (1985) Surface Enhanced Raman Spectroscopic Evidence that Adsorption on Silver Particles Can Denature Heme Proteins. *J. Phys. Chem. 89*, 5168−5173.

(22) Smulevich, G., Mauro, J. M., Fishel, L. A., English, A. M., Kraut, J., and Spiro, T. G. (1988) Cytochrome c Peroxidase Mutant Active Site Structures Probed by Resonance Raman and Infrared Signatures of the CO Adducts. *Biochemistry 27*, 5486−5492.

(23) Sturm, A., Schierhorn, A., Lindenstrauss, U., Lilie, H., and Bruser, T. (2006) YcdB from *Escherichia coli* Reveals a Novel Class of Tat-dependently Translocated Hemoproteins. *J. Biol. Chem. 281*, 13972−13978.

(24) Todorovic, S., Jung, C., Hildebrandt, P., and Murgida, D. (2006) Conformational Transitions and Redox Potential Shifts of Cytochrome P450 Induced by Immobilization. *J. Biol. Inorg. Chem. 11*, 119−127.

(25) Todorovic, S., Verissimo, A., Pereira, M. M., Teixeira, M., Hildebrandt, P., Zebger, I., Wisitruangsakul, N., and Murgida, D. (2008) SERR-Spectroelectrochemical Study of a cbb_3 Oxygen Reductase in a Biomimetic Construct. *J. Phys. Chem. B 112*, 16952−16959.
(26) Goodin, D. B., and McRee, D. E. (1993) The Asp-His-Fe Triad of Cytochrome c Peroxidase Controls the Reduction Potential, Electronic Structure, and Coupling of the Tryptophan Free Radical to Heme. *Biochemistry 32*, 3313−3324.
(27) Ayala, M., Roman, R., and Vazquez-Duhalt, R. (2007) A Catlytic Approach to Estimate the Redox Potential of Heme-peroxidases. *Biochem. Biophys. Res. Commun. 375*, 804−808.
(28) Brown, M. E., Barros, T., and Chang, M. C. Y. (2012) Identification and Characterization of a Multifunctional Dye Peroxidase from a Lignin-Reactive Bacterium. *ACS Chem. Biol. 7*, 2074−2081.
(29) Murgida, D. H., Hildebrandt, P., and Todorovic, S. (2010) Immobilized Redox Proteins: Mimicking Basic Features of Physiological Membranes and Interfaces. In *Biomimetics, learning from nature* (Mukherjee, A., Ed.) pp 21−47, IN-TECH, Vienna.
(30) Todorovic, S., Pereira, M. M., Bandeiras, T. M., Teixeira, M., Hildebrandt, P., and Murgida, D. (2005) Midpoint Potentials of Hemes a and a_3 in the Quinol Oxidase from *Acidianus ambivalens* Are Inverted. *J. Am. Chem. Soc. 127*, 13561−13566.
(31) Todorovic, S., Rodrigues, M. L., Matos, D., and Pereira, I. A. C. (2012) Redox Properties of Lysine- and Methionine- coordinated Hemes Ensure Downhill Electron Transfer in $NrfH_2A_4$ Nitrite Reductase. *J. Phys. Chem. B 116*, 5637−5643.
(32) Sezer, M., Millo, D., Weidinger, I. M., Zebger, I., and Hildebrandt, P. (2012) Analyzing the Catalytic Processes of Immobilized Redox Enzymes by Vibrational Spectroscopies. *IUBMB Life 64*, 455−464.
(33) Santos, A., Mendes, S., Brissos, V., and Martins, L. O. (2013) Comparative study of activity and stability in *Bacillus subtilis* and *Pseudomonas putida* dye decolourizing peroxidases: Towards biotechnological applications. *PLoS One*,.
(34) Dopner, S., Hildebrandt, P., Mauk, A. G., Lenk, H., and Stempfle, W. (1996) Analysis of Vibrational Spectra of Multicomponent Systems. Application to pH-dependent Resonance Raman Spectra of Ferricytochrome *c*. *Spectrochim. Acta, Part A 52*, 573−584.
(35) Siebert, F., and Hildebrandt, P. (2008) *Vibrational Spectroscopy in Life Sciences*, Wiley-VCH Verlag GmbH & Co., Weinheim, Germany.
(36) Maltempo, M. M., Moss, T. H., and Cusanovich, M. A. (1974) Magnetic Studies on the Changes in the Iron Environment in Chromatium Ferricytochrome *c*′. *Biochim. Biophys. Acta 342*, 290−305.
(37) Murgida, D. H., and Hildebrandt, P. (2004) Electron-Transfer Processes of Cytochrome c at Interfaces. New Insights by Surface-Enhanced Resonance Raman Spectroscopy. *Acc. Chem. Res. 37*, 654−661.
(38) Evangelista-Kirkup, R., Crisanti, M., Poulos, T. L., and Spiro, T. G. (1985) Resonance Raman Spectroscopy Shows Different Temperature-dependent Coordination Equilibria for Native Horseradish and Cytochrome *c* Peroxidase. *FEBS Lett. 190*, 221−226.
(39) Chouchane, S., Girotto, S., Kapetanaki, S., Schelvis, J. P. M., Yu, S., and Magliozzo, R. S. (2003) Analysis of Heme Structural Heterogeneity in *Mycobacterium tuberculosis* Catalase Peroxidase (KatG). *J. Biol. Chem. 278*, 8154−8162.
(40) Battistuzzi, G., Borsari, M., Ranieri, A., and Sola, M. (2002) Redox Thermodynamics of the Fe^{3+}/Fe^{2+} Couple in Horseradish Peroxidase and its Cyanide Complex. *J. Am. Chem. Soc. 124*, 26−27.